Global and Planetary Change 261 (2026) 105410

Contents lists available at ScienceDirect

Global and Planetary Change

journal homepage: www.elsevier.com/locate/gloplacha

Research Article

Elevated production and efflux of marine isoprene driven by the atmospheric deposition in the Northwest Pacific Ocean

Jian Wang [a,b], Chengshuai Li [a], Lei Xue [c], Lei Feng [d], Feng Xu [a,e], Jiawei Zhang [f], Chao Zhang [d,*], Honghai Zhang [a,b,*], Zhaohui Chen [g]

[a] Frontiers Science Center for Deep Ocean Multispheres and Earth System, Key Laboratory of Marine Chemistry Theory and Technology, Ministry of Education, and College of Chemistry and Chemical Engineering, Ocean University of China, Qingdao 266100, China
[b] Laoshan Laboratory, Qingdao 266237, China
[c] Department of Chemistry, College of Environmental Science and Forestry, State University of New York, Syracuse, NY 13210, United States
[d] Key Laboratory of Marine Environment and Ecology, Ministry of Education of China, Ocean University of China, Qingdao 266100, China
[e] State Key Joint Laboratory of Environmental Simulation and Pollution Control, International Joint Research Center for Atmospheric Research (IJRC), College of Environmental Sciences and Engineering, Peking University, Beijing 100871, China
[f] Eco-Environmental Monitoring and Research Center, Pearl River Valley and South China Sea Ecology and Environment Administration, Ministry of Ecology and Environment, Guangzhou 510610, China
[g] Key Laboratory of Physical Oceanography, Ministry of Education, Ocean University of China, Qingdao 266100, China

ARTICLE INFO

Editor: Dr. Fabienne Marret-Davies

Keywords:
Atmospheric deposition
Marine isoprene
Biogenic climate-active gas
Sea-to-air flux
Dust-addition experiments

ABSTRACT

Atmospheric deposition is a major external nutrient source to the open ocean and, beyond stimulating primary production, may also enhance the emission of climate-active biogenic gases such as isoprene, introducing additional feedbacks to the Earth system. However, its role in regulating oceanic isoprene production and emissions remains poorly understood. Here, we performed shipboard dust–addition experiments during three cruises in the Northwestern Pacific Ocean (NWPO), in which different dust-addition treatments in a microcosm system (0.1–2.0 mg L^{-1}) were applied to simulate the impact of atmospheric deposition on marine isoprene production. Dust addition significantly stimulated phytoplankton growth and increased isoprene concentrations by 20%–55% relative to the controls. The rise in isoprene was strongly correlated with enhanced Chlorophyll *a* and was further modulated by phytoplankton functional types and nutrient stoichiometry. The largest isoprene enhancement occurred under conditions where phytoplankton communities have high isoprene production rates and N:P ratios of 10–20. The parameterized model based on these experiments predicts that dust deposition raises annual isoprene emissions by 75 ± 17 Gg yr^{-1} in the NWPO. This enhancement likely contributes to regional organic aerosol formation and underscores the potential climate co-benefits of atmospheric deposition through both a strengthened carbon sink and the emission of biogenic cooling agents.

1. Introduction

Atmospheric deposition has become an increasingly important source of nitrogen to the open ocean, with input levels now approaching those of oceanic N_2 fixation (Krishnamurthy et al., 2010). Between 1970 and 2018, global nitrogen deposition to the ocean increased by 89%, largely driven by fossil fuel combustion and intensified fertilizer use (Li et al., 2023; Liu et al., 2023). GEOS-Chem simulations (v12.1.1) estimate an average global oceanic nitrogen deposition of ~40 Tg N yr^{-1}, with 78% occurring in the open ocean (Liu et al., 2025). This external input accounts for around one-third of the non-recycled nitrogen supply and supports ~3% of global annual new marine biological production, equivalent to ~0.3 Gt C yr^{-1}(Duce et al., 2008).

In addition to regulating marine primary productivity, atmospheric deposition could modulate climate change by altering air-sea material exchanges. For example, ~10% of the ocean's drawdown of anthropogenic CO_2 may result from this atmospheric nitrogen fertilization, leading to a decline in radiative forcing (Duce et al., 2008). In parallel, nitrogen-stimulated new production could also increase the emission of biogenic trace gases with climate relevance, thereby introducing additional feedbacks to the Earth system. Among these gases, isoprene—the most abundant volatile organic compound—plays an important role due

* Corresponding authors.
E-mail addresses: zhangchao@ouc.edu.cn (C. Zhang), honghaizhang@ouc.edu.cn (H. Zhang).

https://doi.org/10.1016/j.gloplacha.2026.105410
Received 8 December 2025; Received in revised form 1 March 2026; Accepted 2 March 2026
Available online 4 March 2026

to its climate-active properties. In the open ocean, most atmospheric isoprene originates from phytoplankton production (Bonsang et al., 1992). Once emitted into the atmosphere, isoprene undergoes rapid oxidation with hydroxyl radicals (Berndt et al., 2025) to form secondary organic aerosols (SOA) (Kroll et al., 2006; Palmer and Shaw, 2005), which can potentially serve as cloud condensation nuclei (CCN) (Vallina et al., 2007), thereby enhancing cloud formation and increasing the Earth's albedo (Carslaw et al., 2013; Claeys et al., 2004).

Atmospheric nitrogen deposition in the Northwest Pacific Ocean (NWPO) has increased substantially since the 1980s, rising by 1.0–1.5 times by 2023, with significant implications for regional marine productivity and biogeochemical cycles (Duce et al., 2008; Kim et al., 2011, 2014). However, quantitative constraints on the magnitude of marine isoprene responses to atmospheric nitrogen deposition remain largely lacking. To address this gap, we conducted a series of dust addition experiments in the NWPO to simulate episodic atmospheric deposition and assess its impact on marine isoprene. By integrating experimental results with mechanistic insights, we provide an estimate of nitrogen-driven isoprene response in the NWPO. Collectively, these findings aim to reveal the previously overlooked role of deposited nitrogen in modulating climate-relevant trace gas fluxes over the open ocean.

2. Materials and methods

2.1. Microcosm incubation design

Dust samples used in the onboard microcosm experiments were collected prior to the cruise from either the East China Sea or Qingdao, China (120.49°E, 36.16°N), using a high-volume total suspended particulate sampler (KB-1000, Jinshida Electronic Technology, China). Detailed sampling information is provided in Table S1. Quartz fiber filters (20 × 25 cm) were used for sample collection. All samples were stored at −20 °C in the dark until analysis and experimental use.

A total of five onboard microcosm incubation experiments were conducted in the NWPO aboard the *R/V Dongfanghong 3* during three separate cruises: fall 2019 (station M1), summer 2021 (station M2 and M3), and summer 2023 (station M4 and M5). The locations of the incubation experiments are shown in Fig. 1. Surface seawater was collected from a depth of 5 m using 12 L Niskin bottles mounted on a CTD rosette system (Seabird 911 plus, USA). The seawater was prefiltered through a 200 μm nylon mesh to remove large zooplankton and then distributed into pre-acid-cleaned 20 L polycarbonate bottles.

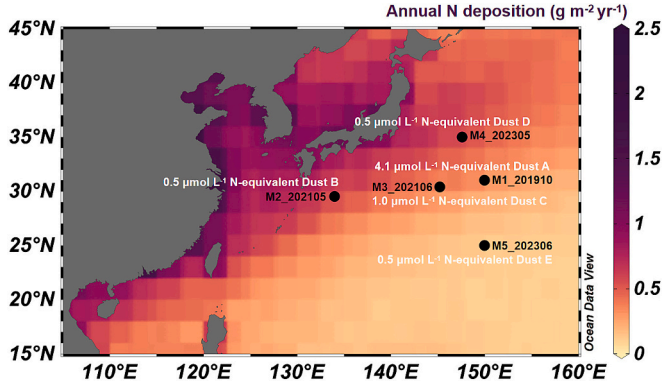

Fig. 1. Locations of the sampling stations for the five microcosm experiments during three cruises in the NWPO. The dust addition in the incubation experiments ranged from 0.10 to 2.0 mg L^{-1}, corresponding to N-equivalent concentrations of 0.5 to 4.1 μmol L^{-1}, as detailed in Table S1. The background color of the map indicates the annual atmospheric nitrogen deposition flux in the Northwest Pacific Ocean in 2023. Data of atmospheric nitrogen deposition flux was obtained from the Inter-Sectoral Impact Model Intercomparison Project (ISIMIP, https://data.isimip.org/, dataset ID: 33080318-7caa-48d1-857a-8a7656474d66 and 5bdb5049-6a6d-4bcc-9f94-2e7af6371099).

Each experiment included a dust addition treatment and a control group, with three replicates per treatment. To ensure a controlled and reproducible representation of atmospheric dust inputs, the water-soluble fraction of dust retained on the filters was extracted with Milli-Q water and directly added to the microcosms. This approach was intended to represent the bioavailable component of atmospheric deposition, which is widely regarded as the most reactive fraction influencing marine biogeochemical processes. The extraction procedure also enabled us to standardize material inputs among treatments and reduce variability associated with particle size distribution and dissolution kinetics in enclosed incubation systems. We note that this method may introduce soluble components more rapidly than occurs under natural deposition conditions, where leaching and dissolution proceed gradually. Therefore, the observed responses should be interpreted primarily as short-term effects of bioavailable dust inputs. The dust-laden filters were extracted in 60 mL of Mili-Q water under ultrasonic agitation for 1 h at 0 °C. For station M1, the final dust concentration was adjusted to 2.0 mg L^{-1} to simulate a case of strong aerosol deposition of 1–6 g m^{-2} into the upper ocean (Zhang et al., 2019). For stations M2-M5, the dust addition concentrations were normalized to total nitrogen equivalents of either 0.5 or 1.0 μmol L^{-1} (Table S1). All incubation bottles were placed in a flow-through tank on the deck, which was continuously supplied with seawater pumped from 5 m depth to maintain ambient temperature conditions. Light intensity was reduced by approximately 40% using neutral density screening, a condition shown to be suitable for deck incubations using 5 m seawater (Guo et al., 2012). Samples were collected in bottles on pre-defined days for the analysis of isoprene, Chl-*a*, nutrients, and phytoplankton community composition. Detailed sampling procedures are described in Supplementary Text S1, and the specific sampling schedule is provided in Table S2.

It is important to note that, although the incubation experiments were designed using realistic atmospheric deposition intensities for the NWPO and included different dust concentration gradients, enclosure-based experiments cannot fully replicate the complexity of natural ocean conditions. In reality, atmospheric deposition can occur very slowly, and such subtle inputs may influence surface isoprene in a gradual and cumulative manner, with effects that are less apparent than those observed under experimental conditions. Nevertheless, our experiments provide important evidence for understanding the responses of isoprene production to varying magnitudes of atmospheric deposition.

2.2. Isoprene analysis

Isoprene concentrations in incubation samples were measured immediately onboard using a purge-and-trap system coupled with a gas chromatograph equipped with a flame ionization detector (GC-FID, 7890B, Agilent, USA). The purge-and-trap system was an optimized version of a previously developed setup (Wang et al., 2023a). Briefly, seawater samples (250 mL) were collected using a custom-made glass bottle connected directly to the inlet of the system. The sample was transferred into an extraction chamber and purged with high-purity N_2 gas at a constant flow rate of 250 mL min^{-1}. Moisture in the purge gas was removed by passing it through a narrow glass condenser housed in a cold chamber maintained at 4–6 °C. CO_2 was scrubbed from the gas stream using a glass tube packed with Ascarite II (Merck, Germany). Isoprene was trapped in a passivated stainless steel tube submerged in liquid nitrogen for 26 min. Then, the trap was rapidly heated in boiling water, and a six-way valve was activated to transfer the sample into the GC-FID for analysis. Separation was performed using an Rt-Alumina BOND/KCl capillary column (50 m × 0.32 mm × 5 μm, Agilent, USA). Details of the inlet, temperature program, and detector settings are provided in Table S3 of the Supporting Information. A certified isoprene gas standard (Linde Gases, Germany) was diluted with high-purity N_2 to 10 parts per billion for calibration. Instrumental blanks were routinely analyzed to verify measurement accuracy. The method yielded a

precision of 3% and a detection limit of 0.5 pmol L^{-1}.

2.3. Environmental parameter analyses

Leachable nutrients, including phosphate (PO_4^{3-}), ammonium (NH_4^+), nitrite (NO_2^-), and nitrate (NO_3^-), were extracted from dust samples by ultrasonication in deionized water at 0 °C for 1 h (Qi et al., 2018). The resulting extracts were filtered through a 0.45 μm PTFE syringe filter and analyzed immediately using a Continuous Flow Analyzer (AA3, SEAL Analytical, Germany) based on standard automated colorimetric methods. The detection limits were 0.02, 0.04, 0.003, and 0.02 μmol L^{-1} for PO_4^{3-}, NH_4^+, NO_2^-, and NO_3^-, respectively. For nutrient analyses in the microcosm seawater, 200 mL of seawater was collected on designated sampling days, filtered through cellulose acetate membranes, and stored in acid-cleaned polyethylene bottles at −20 °C until analysis in the land-based laboratory.

To determine Chl-*a* concentrations, 300 mL of seawater was filtered through 0.2 μm membranes. Pigments retained on the filters were extracted in 90% acetone at −20 °C for 24 h and quantified fluorometrically using a Turner Trilogy fluorometer, with the detection limit and precision of 0.05 μg L^{-1} and 0.5%, respectively.

The phytoplankton community was analyzed by high-throughput sequencing of the V4 region of the 18S rRNA gene. 500 mL seawater was filtered through 0.2 μm polycarbonate membranes, which were subsequently transferred to cryovials and flash-frozen in liquid nitrogen for storage. DNA was extracted from the filters, and the V4 regions of the 18S rRNA gene were amplified using specific primers. Amplicons were sequenced on an Illumina platform. Sequencing data were quality-filtered and denoised, and operational taxonomic units (OTUs) were identified and analyzed using the QIIME2 pipeline. Taxonomic annotation provided detailed profiles of phytoplankton diversity and community structure.

2.4. Statistical analyses

Differences between the dust-added and control groups were assessed using a two-tailed paired-sample *t*-test (SPSS 22.0) to examine whether the mean concentrations of isoprene, Chl-*a*, and nutrients differed significantly over the incubation period. Statistical significance was considered at $p < 0.05$, and the exact *t* and *p* values are provided in Table S4.

3. Results and discussion

3.1. Oceanographic background of the incubation stations in the NWPO

Five microcosm incubation experiments (M1–M5) were conducted using seawater samples collected from the surface of the NWPO during three cruises (Fig. 1). At stations M1–M5, concentrations of dissolved inorganic nitrogen (DIN = $NO_2^- + NO_3^- + NH_4^+$) were 0.040, 0.364, 0.037, 0.010, and 0.045 μmol L^{-1}, respectively, while concentrations of dissolved inorganic phosphorus (DIP) were 0.07, 0.06, 0.08, 0.03, and 0.03 μmol L^{-1} (Table S5). The surface N:P ratios at these stations ranged from 0.33 to 6.1, consistently remaining below the threshold of 10, which is indicative of nitrogen limitation (Maberly et al., 2020). This pattern is consistent with long-term observational studies indicating that nitrogen limitation frequently occurs in open-ocean regions of the NWPO, particularly in oligotrophic waters similar to our study area (Yasunaka et al., 2021). Such low and imbalanced nutrient stoichiometry is known to constrain phytoplankton growth (Klausmeier et al., 2004). Chlorophyll *a* (Chl-*a*) concentrations averaged (± s.d.) 0.161 (± 0.084) μg L^{-1}, ranging from 0.045 to 0.273 μg L^{-1} in the water samples from the surface of these incubation stations. The phytoplankton community was composed of Dinoflagellata, Bacillariophyta, Chlorophyta, Haptophyta, and Cryptophyta. Among these algal phyla, Dinoflagellata was consistently the dominant one, accounting for 36%–86% of the total community (Table S6). This is consistent with a comprehensive taxonomic analysis in the NWPO, where Dinoflagellata was determined to contribute to ~66% of the total algal species diversity (Chen et al., 2021). Surface seawater isoprene concentrations averaged 13.9 ± 5.37 pmol L^{-1} (range 9.05–23.8 pmol L^{-1}; $n = 5$), which aligns well with previous measurements in similar regions. For example, there were comparable values of 14.3 ± 2.41 pmol L^{-1} reported in the Kuroshio Extension region (Wang et al., 2023a) and approximately 17 pmol L^{-1} in the subtropical NWPO (Ooki et al., 2015), respectively.

3.2. Variations of nutrients, Chl-a, and isoprene following dust addition in microcosms

3.2.1. Nutrients

Following dust addition, DIN concentrations in the treatment groups were 1.5–7.6 times higher than those in the corresponding control groups on Day 0. Initial DIN concentrations (mean ± s.d.) in the treatment groups of M2–M5 were 0.929 ± 0.022, 1.367 ± 0.018, 0.357 ± 0.015, and 0.362 ± 0.004 μmol L^{-1}, respectively. Due to a higher dust addition, the initial DIN concentration in M1 reached up to 3.63 ± 0.34 μmol L^{-1}, a level comparable to the input from a strong dust deposition event affecting the upper 10 m of the ocean (Zhang et al., 2019). Unlike the enhanced level of DIN, no significant change in DIP concentrations was observed in either the treatment or control groups. Approximately 50% of DIP measurements fell below the detection limit during the incubation, and the detectable values ranged from 0.02 to 0.08 μmol L^{-1} (Table S7). Dust made only a negligible contribution to seawater DIP relative to its impact on DIN. Despite rapid DIN drawdown, N:P ratios remained above the threshold 16:1 throughout most of the incubation. The N:P ratio in the treatment groups decreased from an initial value of ~60 to ~20 at the termination of the incubation. In contrast, the control group experienced nitrogen limitation for most of the time, with 77% of N:P ratios falling below 16 and a mean value of 6.3 ± 4.2 (Table S7).

3.2.2. Chl-a and phytoplankton

Dust addition elicited a pronounced phytoplankton response, as evidenced by significantly higher Chl-*a* concentrations in the dust-added groups than in the controls ($p \leq 0.001$, Table S4). Across all five microcosm experiments, Chl-*a* concentrations averaged 0.12 ± 0.08 μg L^{-1} in the control groups, whereas dust addition increased them by 50%–150%, resulting in an overall mean of 0.24 ± 0.18 μg L^{-1}. The short-term Chl-*a* dynamics following dust addition varied among stations. In M4, Chl-*a* increased rapidly during the first 4 days, while the other four stations showed more gradual increases. These differences are likely related to the variabilities in initial community composition and the physiological responses of different phytoplankton groups to dust addition. Dinoflagellata dominated the phytoplankton community on Day 0 of the experiment, accounting for 51%–86% in microcosms M2-M5 (Table S6). However, their responses to elevated nitrogen were relatively attenuated under phosphorus-limited conditions (Morey et al., 2011). By contrast, Bacillariophyta, equipped with highly efficient nitrate reductase activity and nitrate transport capacity, exhibited a rapid growth response to elevated nitrogen (Smith et al., 2019). Bacillariophyta already accounted for 12% of the community in M4 on Day 0, compared with <2% in M2, M3, and M5, which likely contributed to the faster increase in Chl-*a* concentration observed at M4. In M1 on Day 0, Bacillariophyta accounted for 61% of the community, and the initial DIN concentration was 3.63 μmol L^{-1}, the highest among all five microcosms; nevertheless, the increase in Chl-*a* was lower than expected. This unexpected response may reflect toxicity associated with the excessive dust addition that was roughly tenfold higher than in M2–M5. Such a large amount of dust could have supplied higher concentrations of toxic heavy metals, such as Cu, Pb, and Cd, which are known to inhibit phytoplankton growth (Miao et al., 2005).

Because dissolved metal concentrations were not directly measured in the incubation systems, Cu input was estimated based on the average

atmospheric Cu concentration (~5 ng m^{-3}) reported for Huaniao Island in the East China Sea (Yang et al., 2020). This value was multiplied by the equivalent filtered air volume represented by the dust mass added to the incubation system and then normalized to the incubation volume. Based on this calculation, the Cu concentration in treatment M1 was estimated to be approximately 0.034 μg L^{-1} following dust addition. This corresponds to a Cu:Chl-*a* ratio of 0.41 μg $μg^{-1}$ in M1, which falls within the toxicity threshold range of 0.2–2 μg $μg^{-1}$ reported by Paytan et al. (2009), suggesting that Cu toxicity may have contributed to the suppressed response of phytoplankton in M1.

3.2.3. Isoprene

In the dust-added groups, the mean isoprene concentrations over the entire incubation period were 14.7 ± 4.8, 24.0 ± 4.47, 16.2 ± 4.55, 21.2 ± 7.89, and 24.2 ± 10.7 pmol L^{-1} in the M1–M5, respectively, which were significantly higher than those in the controls (two-tailed paired-sample *t*-test; exact *p*-values were provided in Table S4). Microbial consumption and physical diffusion are important sinks for isoprene (Simó et al., 2022); however, our experiments did not allow their individual contributions to be quantified. Accordingly, the reported changes in isoprene concentrations reflect the net production within the microcosms. Throughout each incubation, the mean isoprene concentrations in the dust-added groups were 20%–55% higher than those in the control groups, based on the average over the entire incubation period. A marked increase in isoprene concentrations was observed after Day 4 following dust addition, with the average daily increase between Day 4 and the peak day typically ranging from 1.65 to 2.03 pmol L^{-1} d^{-1}. In most cases (M1–M4), isoprene concentrations in the dust-treated groups peaked around Day 8, reaching values between 22.5 and 40.1 pmol L^{-1}. (see Fig. 2) Similarly, it was reported that in the equatorial Pacific (142°E, 3°N), the addition of field-collected aerosol (equivalent to ~6 mg N m^{-2} d^{-1} of atmospheric dry deposition) led to a ~ 70% increase in isoprene concentration compared to controls (Wu et al., 2023).

Although dust addition was the primary driver distinguishing the incubation treatments, isoprene concentrations in the dust-added groups exhibited a significant positive correlation only with Chl-*a* ($r = 0.49$, $p < 0.01$, Fig. 3a). However, isoprene concentrations did not simply scale

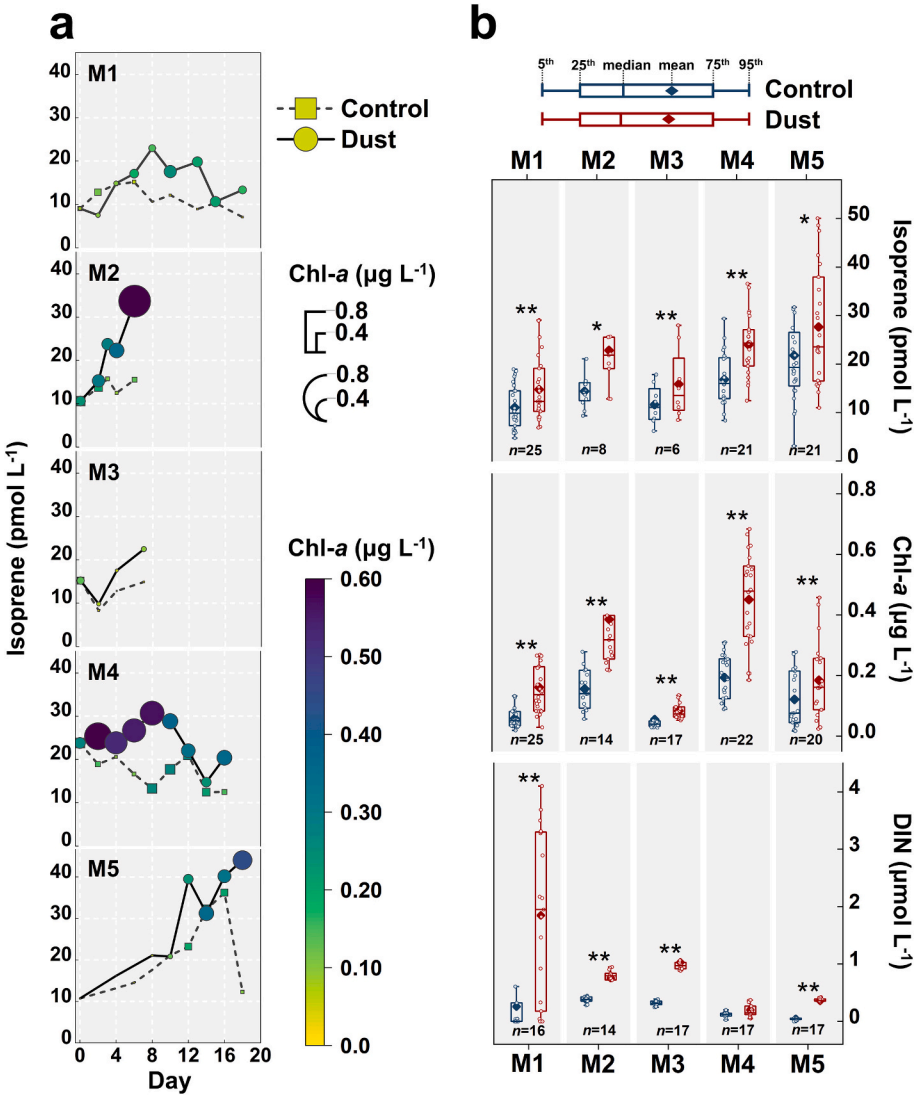

Fig. 2. Responses of isoprene, Chl-*a*, and DIN to dust additions in microcosms. Panel a shows the variations of isoprene concentrations in the control (short-dashed line with squares) and dust-treated (line with dots) groups during the incubations, and the dot/square size and color indicate the corresponding Chl-*a* concentration. Values in panel a are means of three replicates, with standard deviations shown in Fig. S1. Box plots in panel b show the pooled data distribution for each group over the cultivation period. ** and * represent significant differences between control and dust-treated groups at the $p < 0.01$ and $p < 0.05$ levels, respectively, as determined by a two-tailed paired-sample *t*-test. The exact *t* and *p* values are provided in Table S4. Results of M1 have been published in Wang et al. (2023a).

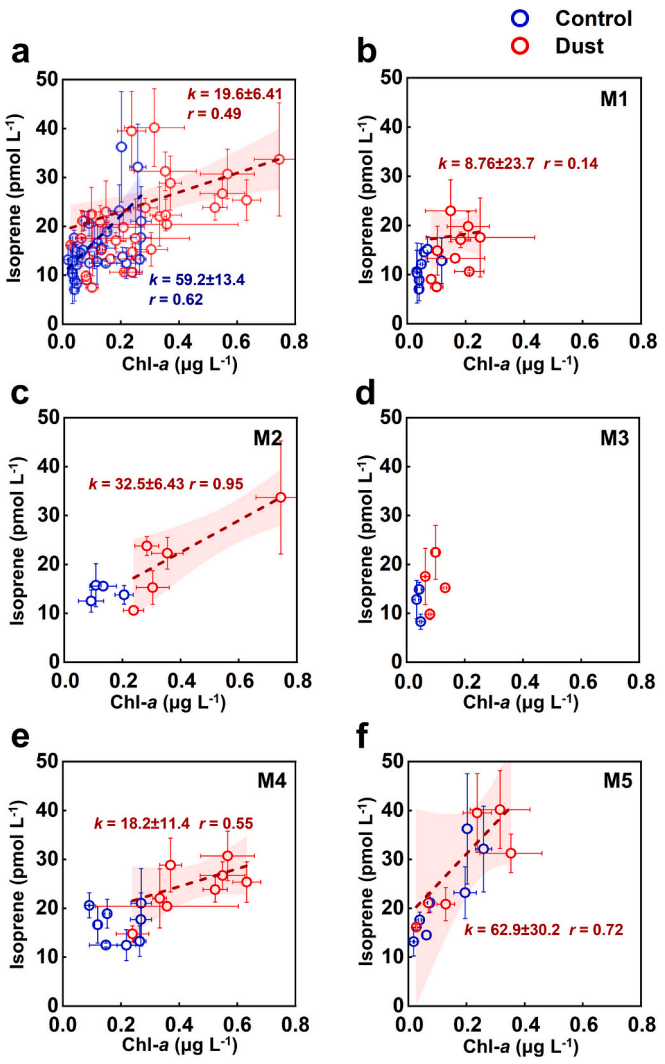

Fig. 3. Linear regression plotting for the concentrations of isoprene and Chl-*a* determined in dust-treated (red-edge dots) and control (blue-edge dots) samples in the five microcosm incubations (M1-M5, panel b-f) in the NWPO. Panel a shows the regression using the data from all the incubations. *k* is the fitted slope, and *r* is the Pearson correlation. Error bars represent the standard deviations from triplicate measurements. Short dashed lines indicate the regression lines, and the shaded areas represent the 95% confidence bands. (For interpretation of the references to color in this figure legend, the reader is referred to the web version of this article.)

with the amount of dust supplied (Fig. S2). This non-linear pattern likely reflects the complex cascade linking dust input to isoprene production, whereby dust influences phytoplankton growth and community composition, which in turn modulate isoprene production. Additional factors, such as heavy metal toxicity (Paytan et al., 2009) and imbalanced nutrient stoichiometry (Chien et al., 2016) under high dust loads, may further attenuate phytoplankton responses. Therefore, accurately quantifying the contribution of dust deposition to marine isoprene budgets requires better constraining the relationship between phytoplankton responses and associated increases in isoprene concentrations under atmospheric deposition scenarios.

3.3. Controlling factors of the coupled isoprene-Chl-a response to dust

Owing to its biogenic origin in the ocean, isoprene concentration has often been linked to Chl-*a*, enabling large-scale mapping using satellite-derived data (Booge et al., 2016; Conte et al., 2020; Cui et al., 2023; Exton et al., 2013; Gantt et al., 2009). In this study, a significant positive correlation was also observed between the dust-driven changes in isoprene and Chl-*a* (Δisoprene vs. ΔChl-*a*) ($r = 0.54$, $p < 0.01$, Fig. S3). To better constrain the model, we examined how Phytoplankton functional types (PFT) and nutrient stoichiometry modulate the isoprene-Chl-*a* relationship under dust perturbations.

3.3.1. Phytoplankton functional type

By including all the data from five microcosms, the slope of the linear regression between isoprene concentration and Chl-*a* in the dust-treated groups ($k_{dust} = 19.6 \pm 6.41$ pmol isoprene/μg Chl-*a*) was lower than that in the controls ($k_{control} = 59.2 \pm 13.4$ pmol isoprene/μg Chl-*a*) (Fig. 3a), indicating a reduced net production of isoprene per unit of Chl-*a* following dust addition. This is likely due to the shifts in phytoplankton community composition following dust addition, as different taxa exhibit markedly different isoprene production rates (Booge et al., 2016). From the beginning to the end of the incubations, the relative abundance of Dinoflagellata in M2–M5 decreased from 66%, 86%, 51%, and 85% to 49%, 15%, 35%, and 46%, respectively (Table S6). Concurrently, the dominant groups shifted to Ochrophytes in M2 (35%) and M5 (45%), to Bacillariophyceae in M4 (67%). Only in M1 did the proportion of Dinoflagellata increase from 36% to 77%. Toxicity assessments based on pulse-amplitude modulated fluorometry have shown that dinoflagellates exhibit greater tolerance to toxic heavy metals than other phytoplankton groups (Miao et al., 2005), which may explain their increased dominance under the potential heavy metal stress associated with the high dust load in M1.

To parameterize phytoplankton-derived isoprene production, we compiled Chlorophyll *a*-normalized isoprene production rates (P_{chloro}) across major phytoplankton phyla from published laboratory cultures (Arnold et al., 2009; Bonsang et al., 2010; Colomb et al., 2008; Exton et al., 2013; Shaw et al., 2010). The means rates were 13.8 ± 7.97, 1.47 ± 1.03, 6.92 ± 5.35, 2.54 ± 1.45, and 9.36 ± 0.72 μmol (g Chl-*a*)$^{-1}$ d^{-1} for Dinoflagellata, Chlorophyta, Haptophyta, Bacillariophyta, and Cryptophyta, respectively (Table S6). The reported standard deviations indicate interspecific variability within each phylum and thus provide a measure of uncertainty in P_{chloro}. Incorporating the phytoplankton community composition determined in our microcosms, we then calculated weighted community-level Chlorophyll *a*-normalized isoprene production rates (P_{PFT}) using eq. (1).

$$P_{PFT} = \sum_{i=1}^{n} P_{chloro-i} \times RP_i \quad (1)$$

Where $P_{chloro-i}$ is P_{chloro} of phytoplankton phyla *i*, RP_i is the relative proportion of phytoplankton phyla *i*, *n* indicates the total phyla of the community in the microcosm. At M2–M5, P_{PFT} decreased from 9.95 ± 5.30, 12.2 ± 6.86, 8.15 ± 4.11, 12.0 ± 6.75 μmol (g Chl-*a*)$^{-1}$ d^{-1} on Day 0 to 3.57 ± 1.42, 9.96 ± 5.64, 4.12 ± 1.62, 6.00 ± 3.10 μmol (g Chl-*a*)$^{-1}$ d^{-1} at the end of the incubations, respectively. This is consistent with the declined regression slope of isoprene vs. Chl-*a* following dust addition. Moreover, the fitted slopes exhibited an exponential increase as a function of the initial P_{PFT} across microcosms (Fig. S4). These results highlight the important role of PFTs in shaping isoprene production and provide empirical support for parameterizing isoprene–Chl-*a* relationships under dust deposition scenarios.

3.3.2. Nutrient stoichiometry

A molar N:P ratio < 10 generally indicates N-limitation, whereas ratios >20 indicate P-limitation (Chorus and Spijkerman, 2021; Maberly et al., 2020). Following this criterion, data from all five microcosms were categorized into three groups depending on varying N:P ratio (0–10, 10–20, and > 20) to examine how nutrient stoichiometry influences the isoprene-Chl-*a* relationship. The regression slope of isoprene vs. Chl-*a* was the highest ($k = 44.8 \pm 14.3$, pmol isoprene/μg Chl-*a*) at the N:P ratio range of 10–20, but declined under N-limitation

($k = 14.9 \pm 10.1$ pmol isoprene/μg Chl-*a*) and P-limitation ($k = 28.5 \pm 8.34$ pmol isoprene/μg Chl-*a*) (Fig. 4). Consistently, underway observation in the Eastern Atlantic Ocean reported different correlations between isoprene and pigments under varying N:P ratios, suggesting the role of nutrient availability in shaping isoprene biogenic production (Zindler et al., 2014). This influence is likely due to the differential responses of specific phytoplankton (e.g., Haptophytes and Dinoflagellates), which are particularly sensitive to changes in nutrient concentrations and stoichiometry (Shaw et al., 2010). Therefore, modeling efforts to evaluate the impact of dust deposition on marine isoprene should explicitly account for regional differentiation in nutrients.

Based on sea surface nutrients data from the European Union-Copernicus Marine Service and atmospheric nitrogen deposition fluxes from the Inter-Sectoral Impact Model Intercomparison Project, atmospheric deposition substantially increased N:P ratios in the NWPO, particularly in the nutrient-poor subtropical region, where N:P ratios rose by more than an order of magnitude relative to in situ seawater values (Fig. 4e). However, this additional nitrogen input did not fundamentally alter the N-limitation of the open ocean, especially within the subtropical gyre, where post-deposition N:P ratios remained below 1 (Fig. 4d). Notably, less than 5% area of the NWPO (~6.2×104 km^2, Fig. S5) falls within the N:P ratio range of 10–20, corresponding to the narrow band between the bold blue and red lines in Fig. 4d, which theoretically represents the region more susceptible to enhanced isoprene levels in response to dust–derived nitrogen input.

3.4. Modeling isoprene response to dust deposition: Empirical parameterizations

The microcosm incubation experiments revealed that atmospheric dust deposition stimulates phytoplankton growth, thereby elevating surface isoprene concentration. Building on these results, we established an empirical model to simulate monthly the response of surface isoprene to atmospheric dust deposition in the NWPO. A robust linear relationship was identified between the dust-induced increases in Chl-*a* and isoprene (Fig. S3). Further analysis (Section 3.2) illustrated that both PFTs and the N:P ratio significantly modulate the slope of this Chl*a*-isoprene relationship. To account for these effects, we introduced two coefficients, β_{PFT} and δ_{NP}, to adjust the slope according to the variability of PFTs and the N:P ratios in the marine environment, as formulated in eq. (2).

$$\Delta\text{isoprene} = K_{isoprene/CHLA} \times \beta_{PFT} \times \delta_{NP} \times \Delta\text{CHLA} \quad (2)$$

Where $K_{isoprene/CHLA}$ indicates the linear slope of isoprene versus Chl-*a* that was derived from all mesocosm incubation data in this study, with a value of 19.8 ± 6.00 pmol isoprene/μg Chl-*a*. It serves as a constant representing the fundamental response of isoprene to Chl-*a* changes under dust influence. Additionally, the linear slopes obtained from multiple incubation experiments exhibited an exponential relationship with P_{PFT} (Fig. S4), which was fitted as eq. (3). The linear regression slope of in situ oceanic isoprene vs. Chl-*a*n under dust deposition scenarios (*k*, pmol isoprene/μg Chl-*a*) was then estimated based on remote sensing PFT (doi:10.48670/moi-00281) using eq. (3). The ratio of *k* to the constant $K_{isoprene/CHLA}$ was used to quantify the effect of PFT, yielding the coefficient β_{PFT} by eq. (4).

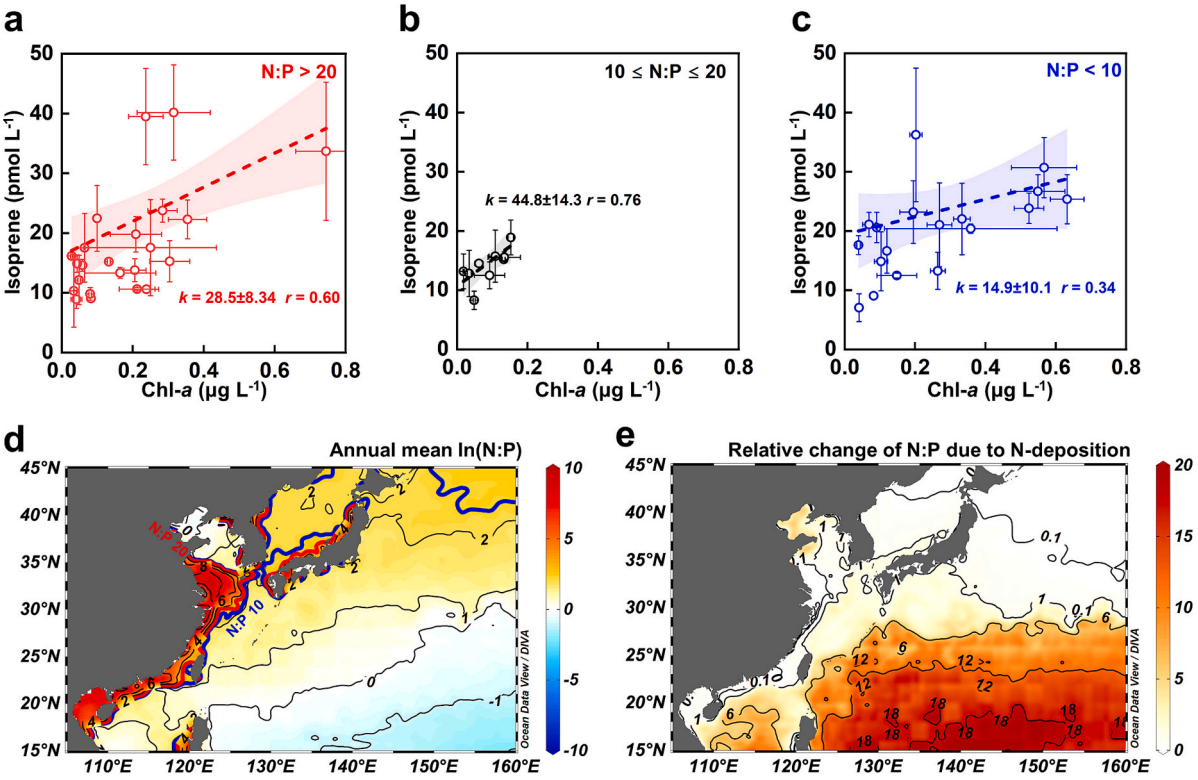

Fig. 4. Effect of N:P ratios on the relationship between isoprene and Chl-*a* concentrations. Linear regressions of isoprene on Chl-*a* at N:P ratios of 1–10 (panel a), 10–20 (panel b), and > 20 (panel c). Error bars represent the standard deviations from triplicate measurements. Short dashed lines indicate the regression lines, and the shaded areas represent the 95% confidence bands. Panel d shows the annual mean N:P ratio in the NWPO in 2023, and the bold blue and red lines represent the N:P ratios of 10 and 20, respectively. Panel e shows the relative change of N:P ratios due to atmospheric nitrogen deposition. Surface nutrient data were downloaded from the European Union-Copernicus Marine Service. (For interpretation of the references to color in this figure legend, the reader is referred to the web version of this article.)

$$k = (0.018 \pm 0.008) \times P_{PFT}^{3.25\pm0.19} \quad (3)$$

$$\beta_{PFT} = \frac{k}{K_{isoprene/CHLA}} \quad (4)$$

δ_{NP} was defined to quantify the effect of the N:P ratio. Specifically, $\delta_{NP} = 1$ when the N:P ratio was between 10 and 20, indicating no nutrient limitation. For N:P ratio < 10 and N:P ratio > 20, corresponding to probable N limitation and P limitation, respectively, δ_{NP} was calculated as the ratio of the slope under the nutrient-limited condition to the slope under the non-limiting condition. Accordingly, δ_{NP} takes values of 0.33 ± 0.25 under N limitation and 0.64 ± 0.28 under P limitation.

Duce et al. (2008) assumed complete assimilation of nitrogen into carbon to estimate the impact of anthropogenic nitrogen deposition on oceanic primary production, an approach we adopted here to quantify the contribution of atmospheric deposition to primary production in the NWPO. The nitrogen flux associated with atmospheric deposition (N_{FLUX}, g m^{-2} $month^{-1}$) was obtained from the Inter-Sectoral Impact Model Intercomparison Project. Using the Redfield ratio, the contribution of N_{FLUX} to primary production (ΔP, g C m^{-2} $month^{-1}$) was calculated according to eq. (5). The classical equation, $P = 1/J_C \times < Chl > \times PAR(0^+) \times \Psi^*$, has been proposed to estimate oceanic primary production from satellite Chl-*a* at the global scale (Antoine et al., 1996), which we adapted to estimate Chl-*a*, as expressed in eq. (6).

$$\Delta P = \frac{N_{FLUX} \times 106}{16} \quad (5)$$

$$\Delta CHLA = \frac{\Delta P \times J_C}{PAR(0^+) \times \Psi^*} \quad (6)$$

where $PAR(0^+)$ is the photosynthetically available radiant energy (400–700 nm) incident at the sea surface per unit area and over a given time interval (e.g., one day J m^{-2}). In this study, we used Aqua MODIS Level 3 Mapped Photosynthetically Available Radiation Data from the NASA Ocean Biology Distributed Active Archive Center. The factor Ψ^* represents the effective photosynthetic cross-section of algae, normalized to areal chlorophyll biomass. A representative mean value of 0.07 ± 0.035 m^2 g Chl-a^{-1}, derived from investigations in oligotrophic Sargasso Sea waters, moderately productive waters in the eastern Equatorial Pacific, and eutrophic waters in the Mauritanian upwelling area (Morel, 1978), is adopted in this study. J_C is the energetic equivalent of photosynthetically fixed carbon (KJ g C^{-1}). The conversion is based on the minimum value of 112 kcal mol^{-1}, corresponding to the reduction of one mole of CO_2 into carbohydrate (CH_2O). Thus, the fixation of 1 mg of carbon is equivalent to an energy storage of 39 J (Morel, 1978).

Having quantified the response of surface isoprene concentrations to the dust deposition, we subsequently estimated the associated sea-to-air flux of isoprene using the two-film model (Wanninkhof, 2014).

$$\Delta F = k_{AS} \times \left([ISO_w] + \Delta isoprene - \frac{[ISO_a]}{H} \right) - k_{AS} \times \left([ISO_w] - \frac{[ISO_a]}{H} \right) = k_{AS} \times \Delta isoprene \quad (7)$$

where $[ISO_w]$ (pmol L^{-1}) is the in situ surface seawater isoprene concentration (pmol L^{-1}), and Δisoprene represents the change in isoprene concentration due to dust addition as evaluated above. $[ISO_a]$ is the atmospheric isoprene concentration, and H is the Henry's law constant for isoprene. k_{AS} (cm h^{-1}) is the gas transfer velocity, the calculation of which is detailed in the Supplementary information.

In summary, we first used the atmospheric nitrogen deposition flux (N_{FLUX}, Fig. S6) to calculate the changes in Chl-*a* (Fig. S7). Based on the distribution of PFT (Fig. S8), we then derived the P_{PFT} (Fig. S9 and Fig. S10), which was further used to evaluate β_{PFT} (Fig. S11 and Fig. S12). Similarly, the surface N:P ratio (Fig. S13) was used to estimate δ_{NP} (Fig. S14 and Fig. S15). These parameters allowed us to calculate the isoprene concentration changes (Fig. S16 and Fig. S17), and ultimately the corresponding sea-to-air fluxes of isoprene (Fig. S18 and Fig. S19). The definitions of the symbols and abbreviations used in the equations are provided in Supplementary Table S8.

3.5. Regional-scale estimation of isoprene response to atmospheric deposition in the NWPO

By integrating the monthly simulation results, we estimated the annual cumulative increase of Chl-*a* and isoprene in the water column attributable to atmospheric deposition during 2023. The model results indicate that dust deposition increased Chl-*a* by an average of 1.7 mg m^{-2} yr^{-1}, with a maximum of 11 mg m^{-2} yr^{-1} occurring in the marginal seas of the NWPO, and declining to approximately 0.1 mg m^{-2} yr^{-1} in the open ocean (Fig. 5c). It should be emphasized that our estimates assume all atmospherically deposited nitrogen is assimilated into carbon, and do not account for the potential inhibitory effects of heavy metals associated with intense dust deposition events (Shi et al., 2012). Therefore, the reported values represent the upper limit of Chl-*a* increase supported by atmospheric deposition. Nevertheless, our results are comparable to previous dust-related simulations in the NWPO (Onitsuka et al., 2009; Taketani et al., 2018; Zhang et al., 2019). For example, simulations using the North Pacific Ecosystem Model coupled with the COCO version 4.9 global ocean circulation model reported that atmospheric nitrogen deposition increased monthly mean Chl-*a* concentrations from 0.15 to 0.25 mg m^{-3} (Zhang et al., 2019). Overall, the upper limit of the annual Chl-*a* increase due to dust deposition across the NWPO in 2023 is estimated to be approximately 29.7 Gg yr^{-1}.

Atmospheric dust deposition was estimated to enhance marine isoprene production on a per-unit sea surface area basis, ranging from 0.02 μg m^{-2} yr^{-1} in the open ocean to 4.8 μg m^{-2} yr^{-1} in shelf regions, with a mean value of 0.40 μg m^{-2} yr^{-1}. These elevated isoprene concentrations resulted in a rise of sea–to–air fluxes by 4.3 mg m^{-2} yr^{-1}, spanning from 0.05 to 34 mg m^{-2} yr^{-1}. For 2023 as a whole, dust deposition increased the total isoprene emissions from the NWPO by 75 ± 17 Gg yr^{-1}, primarily concentrated in coastal regions off China and Japan and in the Kuroshio-Oyashio Extension, where Asian dust transport exerts a strong influence. The dust-induced enhancement in isoprene emissions exhibited a pronounced seasonal cycle, showing a decline-rise trend from January to December (Fig. 5a). The emission increment typically reached its maximum in winter (39.1 Gg) and its minimum in summer (7.1 Gg). This seasonal amplitude was particularly evident in strongly dust-affected regions, such as nearshore waters and areas east of Japan, while the seasonal variability weakened progressively in the subtropical open ocean.

Due to the lack of dust-addition incubation experiments in coastal waters, estimates for these regions were extrapolated from open-ocean experimental results. Moreover, beyond PFTs and nutrient stoichiometry, other environmental factors such as temperature (Exton et al., 2013; Ooki et al., 2015) and light intensity (Gantt et al., 2009) are also known to influence isoprene production rates. However, due to the data limitation, the atmospheric deposition scenario in our model did not account for such variable effects on the isoprene–Chl-*a* relationship. We therefore acknowledge these as additional potential sources of uncertainty.

Despite these limitations, our findings demonstrate that atmospheric dust deposition substantially enhances isoprene emissions in the NWPO. A 20-year (2001−2020) global hourly dataset for marine isoprene emissions suggests that the annual isoprene emission from the Pacific Ocean is 543 Gg yr^{-1} (Cui et al., 2023). Compared with this baseline, East Asian dust input could increase the Pacific isoprene fluxes by up to 14%. Such an enhancement may play a non-negligible role in promoting the formation of regional secondary organic aerosols, such as organosulfates (Wang et al., 2023b). The potential contribution to SOA formation was estimated using the secondary organic aerosol formation

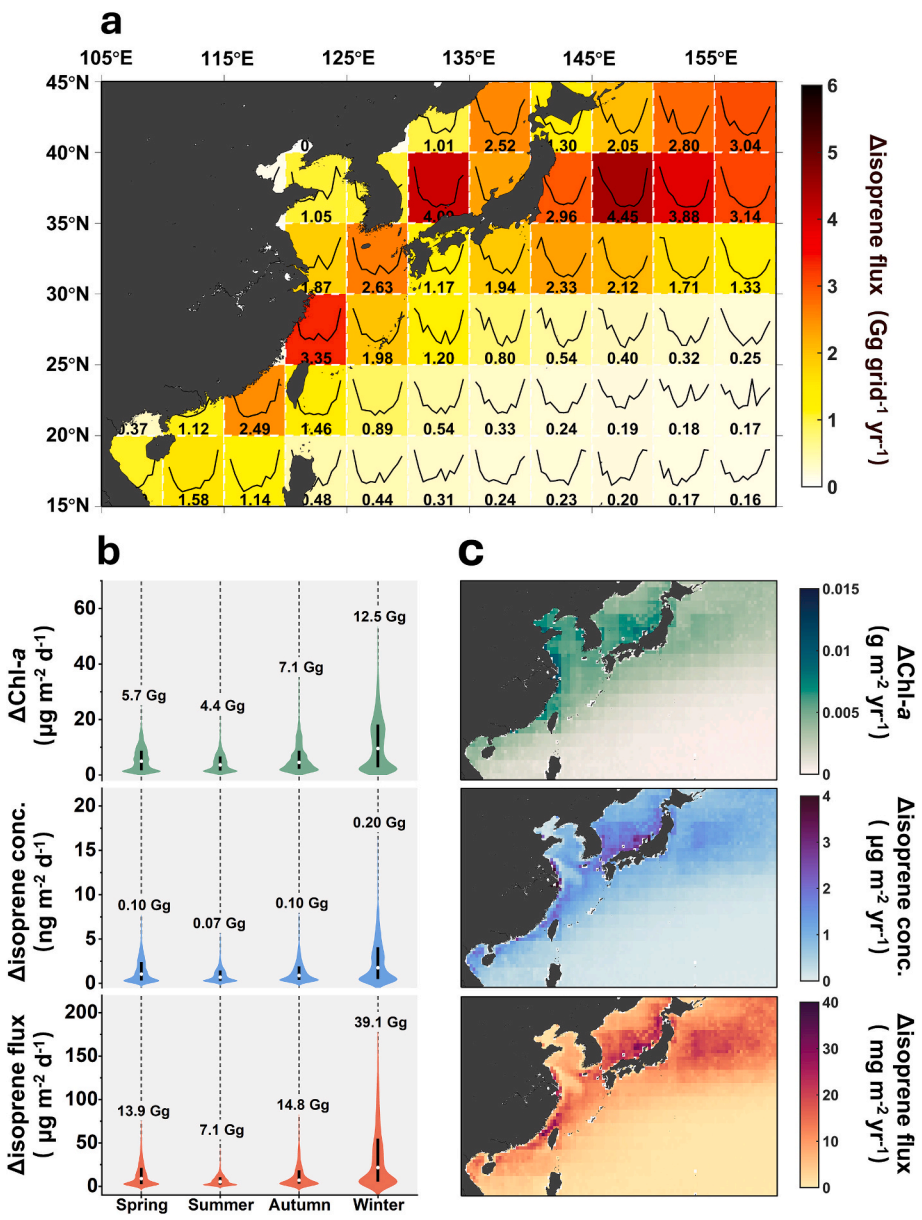

Fig. 5. Simulated results of oceanic isoprene emissions driven by atmospheric deposition. Panel a shows the annual increase in isoprene emissions within each 5° × 5° grid cell, indicated by both numbers and color shading in units of Gg grid^{-1} yr^{-1}. The black curves within each grid depict the normalized monthly variation of isoprene flux from January to December, highlighting the seasonal pattern within individual grid cells. Panel b shows the seasonal comparison of deposition-induced changes in Chl-*a*, isoprene concentration, and isoprene flux over the NWPO. Numbers indicate the total change across the region for each season. Panel c shows the distribution of deposition-induced variations in Chl-*a*, isoprene concentration, and isoprene flux throughout the year.

potential (SOAP) of isoprene relative to toluene ($SOAP = 1.9$; Derwent et al., 2010) and the fractional aerosol coefficient of toluene ($FAC_{toluene} = 5.4\%$; Grosjean and Seinfeld, 1989), following eq. (8) in Zhang et al. (2017). Based on this approach, the dust-induced enhancement in isoprene emissions (ΔF) was estimated to contribute approximately 0.08 $\pm$ 0.02 Gg yr^{-1} of SOA.

$$P_{SOAP} = \Delta F \times SOAP \times FAC_{toluene}/100 \quad (8)$$

Importantly, isoprene is not the only marine biogenic gas with potential climate-cooling effects; other compounds, such as dimethyl sulfide (Charlson et al., 1987) and terpenes (Claeys et al., 2007), could contribute in similar ways. Dust-stimulated phytoplankton growth may therefore simultaneously increase the emissions of multiple climate-active gases. In addition to enhancing oceanic primary production and CO_2 uptake, atmospheric deposition could synergistically strengthen the release of cooling-relevant trace gases, thereby potentially contributing to the mitigation of global warming.

4. Conclusions

In this study, shipboard dust-addition experiments conducted during three cruises in the NWPO suggest that atmospheric deposition may substantially enhance the production and efflux of marine isoprene. Dust inputs consistently stimulated phytoplankton biomass, leading to marked increases in isoprene concentrations. The magnitude of this response was closely linked to phytoplankton community structure and nutrient stoichiometry, especially in assemblages characterized by high intrinsic isoprene productivity and moderate N:P ratios. By integrating experimental results into a parameterized regional model, we estimate that atmospheric deposition increases annual isoprene emissions by 75 $\pm$ 17 Gg yr^{-1} in the NWPO. Such an enhancement may contribute to the

formation of organic aerosols and reinforces the potential role of atmospheric deposition as a climate-modulating process, not only through strengthening oceanic CO_2 uptake but also through stimulating the release of biogenic cooling agents. Our findings highlight the importance of incorporating dust-driven biogeochemical responses into regional and global models to better assess future climate feedbacks in a changing Earth system.

CRediT authorship contribution statement

Jian Wang: Visualization, Supervision, Methodology, Investigation, Data curation, Conceptualization, Writing – review & editing, Writing – original draft. **Chengshuai Li:** Methodology, Investigation. **Lei Xue:** Visualization, Writing – review & editing. **Lei Feng:** Methodology, Investigation. **Jiawei Zhang:** Supervision, Investigation. **Chao Zhang:** Methodology, Investigation, Conceptualization, Writing – review & editing. **Honghai Zhang:** Visualization, Supervision, Methodology, Funding acquisition, Conceptualization, Writing – review & editing. **Zhaohui Chen:** Supervision, Funding acquisition, Conceptualization, Writing – review & editing. **Feng Xu:** Writing – review & editing.

Declaration of competing interest

The authors declare that they have no known competing financial interests or personal relationships that could have appeared to influence the work reported in this paper.

Acknowledgments

We thank the chief scientist, captain, and crews of the R/V Dong Fang Hong 3, as well as our collaborators for their assistance in sampling and analysis during the cruises. This study was supported by the National Natural Science Foundation of China (42276042, 42576041, and 42506044), the Laoshan Laboratory (LSKJ 202400202 and LSKJ 202201701), the Fundamental Research Funds for the Central Universities (202372001, 202072001, and 842513018), and the General Program of China Postdoctoral Science Foundation (2025M770876).

Appendix A. Supplementary data

Supplementary data to this article can be found online at https://doi.org/10.1016/j.gloplacha.2026.105410.

Data availability

Data and code are publicly available on Figshare via doi:https://doi.org/10.6084/m9.figshare.30360055 (Wang, 2025). The remote sensing and reanalysis data used in this study are as follows: Surface nutrient data were sourced from the Global Ocean Biogeochemistry Analysis and Forecast via European Union-Copernicus Marine Service (DOI:10.48670/moi-00015), while atmospheric nitrogen deposition flux was obtained from the Inter-Sectoral Impact Model Intercomparison Project (ISIMIP, https://data.isimip.org/, dataset ID: 33080318-7caa-48d1-857a-8a7656474d66 and 5bdb5049-6a6d-4bcc-9f94-2e7af6371099). PFT data are sourced from Global Ocean Colour (Copernicus-GlobColour), Bio-Geo-Chemical, L4 (monthly and interpolated) from Satellite Observations (1997-ongoing) (DOI:10.48670/moi-00281). PAR data are sourced from NASA Ocean Biology Distributed Active Archive Center, Aqua MODIS Level 3 Mapped Photosynthetically Available Radiation Data, Version R2022.0 (DOI: https://doi.org/10.5067/AQUA/MODIS/L3M/PAR/2022). Data of monthly averaged 10 m wind speed and surface seawater temperature are sourced from ERA5 reanalysis data (DOI:10.24381/cds.f17050d7).

References

Antoine, D., André, J.-M., Morel, A., 1996. Oceanic primary production: 2. Estimation at global scale from satellite (Coastal Zone Color Scanner) chlorophyll. Glob. Biogeochem. Cycles 10, 57–69. https://doi.org/10.1029/95GB02832.

Arnold, S.R., Spracklen, D.V., Williams, J., Yassaa, N., Sciare, J., Bonsang, B., Gros, V., Peeken, I., Lewis, A.C., Alvain, S., 2009. Evaluation of the global oceanic isoprene source and its impacts on marine organic carbon aerosol. Atmos. Chem. Phys. 9, 1253–1262. https://doi.org/10.5194/acp-9-1253-2009.

Berndt, T., Hoffmann, E.H., Tilgner, A., Herrmann, H., 2025. Highly oxidized products from the atmospheric reaction of hydroxyl radicals with isoprene. Nat. Commun. 16. https://doi.org/10.1038/s41467-025-57336-1.

Bonsang, B., Polle, C., Lambert, G., 1992. Evidence for marine production of isoprene. Geophys. Res. Lett. 19, 1129–1132. https://doi.org/10.1029/92GL00083.

Bonsang, B., Gros, V., Peeken, I., Yassaa, N., Bluhm, K., Zoellner, E., Sarda-Esteve, R., Williams, J., 2010. Isoprene emission from phytoplankton monocultures: the relationship with chlorophyll-*a*, cell volume and carbon content. Environ. Chem. 7, 554–563. https://doi.org/10.1071/EN09156.

Booge, D., Marandino, C.A., Schlundt, C., Palmer, P.I., Schlundt, M., Atlas, E.L., Bracher, A., Saltzman, E.S., Wallace, D.W.R., 2016. Can simple models predict large-scale surface ocean isoprene concentrations? Atmos. Chem. Phys. 16, 11807–11821. https://doi.org/10.5194/acp-16-11807-2016.

Carslaw, K.S., Lee, L.A., Reddington, C.L., Pringle, K.J., Rap, A., Forster, P.M., Mann, G. W., Spracklen, D.V., Woodhouse, M.T., Regayre, L.A., Pierce, J.R., 2013. Large contribution of natural aerosols to uncertainty in indirect forcing. Nature 503, 67–71. https://doi.org/10.1038/nature12674.

Charlson, R.J., Lovelock, J.E., Andreae, M.O., Warren, S.G., 1987. Oceanic phytoplankton, atmospheric Sulphur, cloud albedo and climate. Nature 326, 655–661. https://doi.org/10.1038/326655a0.

Chen, Z., Sun, J., Chen, D., Wang, S., Yu, H., Chen, H., Wang, M., 2021. Effects of Ocean Currents in the Western Pacific Ocean on Net-Phytoplankton Community Compositions. Diversity. https://doi.org/10.3390/d13090428.

Chien, C.-T., Mackey, K.R.M., Dutkiewicz, S., Mahowald, N.M., Prospero, J.M., Paytan, A., 2016. Effects of African dust deposition on phytoplankton in the western tropical Atlantic Ocean off Barbados. Glob. Biogeochem. Cycles 30, 716–734. https://doi.org/10.1002/2015GB005334.

Chorus, I., Spijkerman, E., 2021. What Colin Reynolds could tell us about nutrient limitation, N:P ratios and eutrophication control. Hydrobiologia 848, 95–111. https://doi.org/10.1007/s10750-020-04377-w.

Claeys, M., Graham, B., Vas, G., Wang, W., Vermeylen, R., Pashynska, V., Cafmeyer, J., Guyon, P., Andreae, M.O., Artaxo, P., Maenhaut, W., 2004. Formation of secondary organic aerosols through photooxidation of isoprene. Science 303 (80), 1173–1176. https://doi.org/10.1126/science.1092805.

Claeys, M., Szmigielski, R., Kourtchev, I., Van der Veken, P., Vermeylen, R., Maenhaut, W., Jaoui, M., Kleindienst, T.E., Lewandowski, M., Offenberg, J.H., Edney, E.O., 2007. Hydroxydicarboxylic acids:: Markers for secondary organic aerosol from the photooxidation of α-pinene. Environ. Sci. Technol. 41, 1628–1634. https://doi.org/10.1021/es062018.

Colomb, A., Yassaa, N., Williams, J., Peeken, I., Lochte, K., 2008. Screening volatile organic compounds (VOCs) emissions from five marine phytoplankton species by head space gas chromatography/mass spectrometry (HS-GC/MS). J. Environ. Monit. 10, 325–330. https://doi.org/10.1039/b715312k.

Conte, L., Szopa, S., Aumont, O., Gros, V., Bopp, L., 2020. Sources and Sinks of Isoprene in the Global Open Ocean: simulated patterns and Emissions to the Atmosphere. J. Geophys. Res. Ocean. 125. https://doi.org/10.1029/2019JC015946.

Cui, L.H., Xiao, Y.T., Hu, W., Song, L., Wang, Y.J., Zhang, C., Fu, P.Q., Zhu, J.L., 2023. Enhanced dataset of global marine isoprene emissions from biogenic and photochemical processes for the period 2001-2020. Earth Syst. Sci. Data 15, 5403–5425. https://doi.org/10.5194/essd-15-5403-2023.

Derwent, R.G., Jenkin, M.E., Utembe, S.R., Shallcross, D.E., Murrells, T.P., Passant, N.R., 2010. Secondary organic aerosol formation from a large number of reactive man-made organic compounds. Sci. Total Environ. 408 (16), 3374–3381. https://doi.org/10.1016/j.scitotenv.2010.04.013.

Duce, R.A., LaRoche, J., Altieri, K., Arrigo, K.R., Baker, A.R., Capone, D.G., Cornell, S., Dentener, F., Galloway, J., Ganeshram, R.S., Geider, R.J., Jickells, T., Kuypers, M.M., Langlois, R., Liss, P.S., Liu, S.M., Middelburg, J.J., Moore, C.M., Nickovic, S., Oschlies, A., Pedersen, T., Prospero, J., Schlitzer, R., Seitzinger, S., Sorensen, L.L., Uematsu, M., Ulloa, O., Voss, M., Ward, B., Zamora, L., 2008. Impacts of atmospheric anthropogenic nitrogen on the open ocean. Science 320 (80), 893–897. https://doi.org/10.1126/science.1150369.

Exton, D.A., Suggett, D.J., McGenity, T.J., Steinke, M., 2013. Chlorophyll-normalized isoprene production in laboratory cultures of marine microalgae and implications for global models. Limnol. Oceanogr. 58, 1301–1311. https://doi.org/10.4319/lo.2013.58.4.1301.

Gantt, B., Meskhidze, N., Kamykowski, D., 2009. A new physically-based quantification of marine isoprene and primary organic aerosol emissions. Atmos. Chem. Phys. 9, 4915–4927. https://doi.org/10.5194/acp-9-4915-2009.

Grosjean, D., Seinfeld, J.H., 1989. Parameterization of the formation potential of secondary organic aerosols. Atmos. Environ. 23, 1733–1747. https://doi.org/10.1016/0004-6981(89)90058-9.

Guo, C., Yu, J., Ho, T.Y., Wang, L., Song, S., Kong, L., Liu, H., 2012. Dynamics of phytoplankton community structure in the South China Sea in response to the East Asian aerosol input. Biogeosciences 9, 1519–1536. https://doi.org/10.5194/bg-9-1519-2012.

Kim, T.W., Lee, K., Najjar, R.G., Jeong, H.D., Jeong, H.J., 2011. Increasing N abundance in the Northwestern Pacific Ocean due to atmospheric nitrogen deposition. Science 334 (80), 505–509. https://doi.org/10.1126/science.1206583.

Kim, I.N., Lee, K., Gruber, N., Karl, D.M., Bullister, J.L., Yang, S., Kim, T.W., 2014. Increasing anthropogenic nitrogen in the North Pacific Ocean. Science 346 (80), 1102–1106. https://doi.org/10.1126/science.1258396.

Klausmeier, C.A., Litchman, E., Levin, S.A., 2004. Phytoplankton growth and stoichiometry under multiple nutrient limitation. Limnol. Oceanogr. 49, 1463–1470. https://doi.org/10.4319/lo.2004.49.4_part_2.1463.

Krishnamurthy, A., Moore, J.K., Mahowald, N., Luo, C., Zender, C.S., 2010. Impacts of atmospheric nutrient inputs on marine biogeochemistry. J. Geophys. Res. 115. https://doi.org/10.1029/2009JG001115.

Kroll, J.H., Ng, N.L., Murphy, S.M., Flagan, R.C., Seinfeld, J.H., 2006. Secondary organic aerosol formation from isoprene photooxidation. Environ. Sci. Technol. 40, 1869–1877. https://doi.org/10.1021/es0524301.

Li, T., Li, J., Sun, Z., Jiang, H., Tian, C., Zhang, G., 2023. High contribution of anthropogenic combustion sources to atmospheric inorganic reactive nitrogen in South China evidenced by isotopes. Atmos. Chem. Phys. 23, 6395–6407. https://doi.org/10.5194/acp-23-6395-2023.

Liu, L., Xu, W., Wen, Z., Liu, P., Xu, H., Liu, S., Lu, X.K., Zhong, B.Q., Guo, Y.X., Lu, X., Zhao, Y.H., Zhang, X.Y., Wang, S.H., Vitousek, P.M., Liu, X.J., 2023. Modeling global oceanic nitrogen deposition from food systems and its mitigation potential by reducing overuse of fertilizers. Proc. Natl. Acad. Sci. USA 120. https://doi.org/10.1073/pnas.2221459120.

Liu, S., Zhao, Y., Lin, Y., Wang, J., Li, Q., Chen, Y., Zhang, L., 2025. Atmospheric reactive nitrogen deposition to the Global Ocean during the 2010s: interannual variation and source attribution. J. Geophys. Res. Atmos. 130, e2024JD042789. https://doi.org/10.1029/2024JD042789.

Maberly, S.C., Pitt, J.A., Davies, P.S., Carvalho, L., 2020. Nitrogen and phosphorus limitation and the management of small productive lakes. Inland Waters 10, 159–172. https://doi.org/10.1080/20442041.2020.1714384.

Miao, A.J., Wang, W.X., Juneau, P., 2005. Comparison of Cd, Cu, and Zn toxic effects on four marine phytoplankton by pulse-amplitude-modulated fluorometry. Environ. Toxicol. Chem. 24, 2603–2611. https://doi.org/10.1897/05-009R.1.

Morel, A., 1978. Available, usable, and stored radiant energy in relation to marine photosynthesis. Deep-Sea Res. 25, 673–688. https://doi.org/10.1016/0146-6291(78)90623-9.

Morey, J.S., Monroe, E.A., Kinney, A.L., Beal, M., Johnson, J.G., Hitchcock, G.L., Van Dolah, F.M., 2011. Transcriptomic response of the red tide dinoflagellate, Karenia brevis, to nitrogen and phosphorus depletion and addition. BMC Genomics 12, 346. https://doi.org/10.1186/1471-2164-12-346.

Onitsuka, G., Uno, I., Yanagi, T., Yoon, J.H., 2009. Modeling the effects of atmospheric nitrogen input on biological production in the Japan Sea. J. Oceanogr. 65, 433–438. https://doi.org/10.1007/s10872-009-0038-4.

Ooki, A., Nomura, D., Nishino, S., Kikuchi, T., Yokouchi, Y., 2015. A global-scale map of isoprene and volatile organic iodine in surface seawater of the Arctic, Northwest Pacific, Indian, and Southern Oceans. J. Geophys. Res. Ocean. 120, 4108–4128. https://doi.org/10.1002/2014JC010519.

Palmer, P.I., Shaw, S.L., 2005. Quantifying global marine isoprene fluxes using MODIS chlorophyll observations. Geophys. Res. Lett. 32. https://doi.org/10.1029/2005GL022592.

Paytan, A., Mackey, K.R.M., Chen, Y., Lima, I.D., Doney, S.C., Mahowald, N., Labiosa, R., Postf, A.F., 2009. Toxicity of atmospheric aerosols on marine phytoplankton. Proc. Natl. Acad. Sci. USA 106, 4601–4605. https://doi.org/10.1073/pnas.0811486106.

Qi, J.H., Liu, X.H., Yao, X.H., Zhang, R.F., Chen, X.J., Lin, X.H., Gao, H.W., Liu, R.H., 2018. The concentration, source and deposition flux of ammonium and nitrate in atmospheric particles during dust events at a coastal site in northern China. Atmos. Chem. Phys. 18, 571–586. https://doi.org/10.5194/acp-18-571-2018.

Shaw, S.L., Gantt, B., Meskhidze, N., 2010. Production and emissions of marine isoprene and monoterpenes: a review. Adv. Meteorol. 2010. https://doi.org/10.1155/2010/408696.

Shi, J.H., Gao, H.W., Zhang, J., Tan, S.C., Ren, J.L., Liu, C.G., Liu, Y., Yao, X., 2012. Examination of causative link between a spring bloom and dry/wet deposition of Asian dust in the Yellow Sea, China. J. Geophys. Res. Atmos. 117. https://doi.org/10.1029/2012JD017983.

Simó, R., Cortés-Greus, P., Rodríguez-Ros, P., Masdeu-Navarro, M., 2022. Substantial loss of isoprene in the surface ocean due to chemical and biological consumption. Commun. Earth Environ. 3. https://doi.org/10.1038/s43247-022-00352-6.

Smith, S.R., Dupont, C.L., McCarthy, J.K., Broddrick, J.T., Oborník, M., Horák, A., Füssy, Z., Cihlář, J., Kleessen, S., Zheng, H., McCrow, J.P., Hixson, K.K., Araújo, W. L., Nunes-Nesi, A., Fernie, A., Nikoloski, Z., Palsson, B.O., Allen, A.E., 2019. Evolution and regulation of nitrogen flux through compartmentalized metabolic networks in a marine diatom. Nat. Commun. 10, 4552. https://doi.org/10.1038/s41467-019-12407-y.

Taketani, F., Aita, M.N., Yamaji, K., Sekiya, T., Ikeda, K., Sasaoka, K., Hashioka, T., Honda, M.C., Matsumoto, K., Kanaya, Y., 2018. Seasonal response of North Western Pacific marine ecosystems to deposition of atmospheric inorganic nitrogen compounds from East Asia. Sci. Rep. 8. https://doi.org/10.1038/s41598-018-27523-w.

Vallina, S.M., Simó, R., Gassó, S., de Boyer-Montégut, C., del Río, E., Jurado, E., Dachs, J., 2007. Analysis of a potential "solar radiation dose–dimethylsulfide–cloud condensation nuclei" link from globally mapped seasonal correlations. Glob. Biogeochem. Cycles 21. https://doi.org/10.1029/2006GB002787.

Wang, J., 2025. Data and code for "Elevated production and efflux of marine isoprene driven by the atmospheric deposition in the Northwest Pacific Ocean". Figshare [data set]. https://doi.org/10.6084/m9.figshare.30360055.

Wang, J., Zhang, H.H., Booge, D., Zhang, Y.Q., Li, X.J., Wu, Y.C., Zhang, J.W., Chen, Z. H., 2023a. Isoprene production and its driving factors in the Northwest Pacific Ocean. Glob. Biogeochem. Cycles 37. https://doi.org/10.1029/2023GB007841.

Wang, Y., Zhang, Y., Li, W., Wu, G., Qi, Y., Li, S., Zhu, W., Yu, J.Z., Yu, X., Zhang, H.-H., Sun, J., Wang, W., Sheng, L., Yao, X., Gao, H., Huang, C., Ma, Y., Zhou, Y., 2023b. Important roles and formation of atmospheric organosulfates in marine organic aerosols: influence of phytoplankton emissions and anthropogenic pollutants. Environ. Sci. Technol. 57, 10284–10294. https://doi.org/10.1021/acs.est.3c01422.

Wanninkhof, R., 2014. Relationship between wind speed and gas exchange over the ocean revisited. Limnol. Oceanogr. 12, 351–362. https://doi.org/10.4319/lom.2014.12.351.

Wu, Y.C., Gao, X.X., Zhang, H.H., Liu, Y.Z., Wang, J., Xu, F., Zhang, G.L., Chen, Z.H., 2023. Characteristics and emissions of isoprene and other non-methane hydrocarbons in the Northwest Pacific Ocean and responses to atmospheric aerosol deposition. Sci. Total Environ. 876. https://doi.org/10.1016/j.scitotenv.2023.162808.

Yang, T.J., Chen, Y., Zhou, S.Q., Li, H.W., Wang, F.H., Zhu, Y.C., 2020. Solubilities and deposition fluxes of atmospheric Fe and Cu over the Northwest Pacific and its marginal seas. Atmos. Environ. 239. https://doi.org/10.1016/j.atmosenv.2020.117763.

Yasunaka, S., Mitsudera, H., Whitney, F., Nakaoka, S., 2021. Nutrient and dissolved inorganic carbon variability in the North Pacific. J. Oceanogr. 77, 3–16. https://doi.org/10.1007/s10872-020-00561-7.

Zhang, Z., Wang, H., Chen, D., Li, Q., Thai, P., Gong, D., Li, Y., Zhang, C., Gu, Y., Zhou, L., Morawska, L., Wang, B., 2017. Emission characteristics of volatile organic compounds and their secondary organic aerosol formation potentials from a petroleum refinery in Pearl River Delta, Chin. Sci. Total Environ. 584-585, 1162–1174. https://doi.org/10.1016/j.scitotenv.2017.01.179.

Zhang, C., Ito, A., Shi, Z., Aita, M.N., Yao, X., Chu, Q., Shi, J., Gong, X., Gao, H., 2019. Fertilization of the Northwest Pacific Ocean by East Asia Air Pollutants. Glob. Biogeochem. Cycles 33, 690–702. https://doi.org/10.1029/2018GB006146.

Zindler, C., Marandino, C.A., Bange, H.W., Schütte, F., Saltzman, E.S., 2014. Nutrient availability determines dimethyl sulfide and isoprene distribution in the eastern Atlantic Ocean. Geophys. Res. Lett. 41, 3181–3188. https://doi.org/10.1002/2014GL059547.